Structural aspects of elastic deformation of a metallic glass

T. C. Hufnagel* and R. T. Ott†
Department of Materials Science and Engineering, Johns Hopkins University, Baltimore, Maryland 21218-2681, USA

J. Almer
Advanced Photon Source, Argonne National Laboratory, Argonne, Illinois 60439, USA
(Received 1 November 2005; published 21 February 2006)

We report the use of high-energy x-ray scattering to measure strain in a $Zr_{57}Ti_5Cu_{20}Ni_8Al_{10}$ bulk metallic glass *in situ* during uniaxial compression in the elastic regime up to stresses of approximately 60% of the yield stress. The strains extracted in two ways—directly from the normalized scattering data and from the pair correlation functions—are in good agreement with each other for length scales greater than 4 Å. The elastic modulus calculated on the basis of this strain is in good agreement with that reported for closely related amorphous alloys based on macroscopic measurements. The strain measured for atoms in the nearest-neighbor shell, however, is smaller than that for more distant shells, and the effective elastic modulus calculated from the strain on this scale is therefore larger, comparable to crystalline alloys of similar composition. These observations are in agreement with previously proposed models in which the nominally elastic deformation of a metallic glass has a significant anelastic component due to atomic rearrangements in topologically unstable regions of the structure. We also observe that the distribution of the atomic-level stresses in the glass becomes more uniform during loading. This implies that the stiffness of metallic glasses may have an entropic contribution, analogous to the entropic contribution in rubber elasticity.

DOI: 10.1103/PhysRevB.73.064204 PACS number(s): 81.05.Kf, 62.20.Dc, 61.10.Eq

I. INTRODUCTION

X-ray and neutron diffraction are commonly used to measure elastic strains in crystalline materials.[1,2] Elastic strain alters the spacing of atomic planes, which can be measured by diffraction according to Bragg's law. By varying the direction of the scattering vector, d spacings in various directions can be measured and the complete elastic strain tensor determined. The stress tensor can then be determined by application of Hooke's law if the elastic constants of the material are known.

Scattering techniques are also used to study the structure of amorphous materials, including metallic glasses. The accuracy and precision of scattering measurements from amorphous materials, however, are limited by the inherent structural disorder, by time-consuming data collection, and by significant challenges in properly analyzing the data once collected. For these reasons, it has been commonly assumed that the resolution of scattering techniques is insufficient to allow accurate measurement of elastic strain in amorphous materials.

Recently, however, Poulsen and co-workers[3] have shown (for a $Mg_{60}Cu_{30}Y_{10}$ bulk metallic glass) that it is possible not only to measure strain in cylinders under uniaxial compression, but to map the strain distribution in a plate containing a through-thickness hole. Remarkably, they also reported that the measured strain (and thus the elastic constants) depends strongly on the length scale of the measurement, the material being much stiffer for measurements on the atomic scale (2–3 Å) than on longer length scales (4–10 Å). Poulsen and co-workers postulated that this additional compliance results from structural rearrangements on these longer length scales.

In this work, we report our own strain measurements using high-energy x-ray scattering on bulk amorphous $Zr_{57}Ti_5Cu_{20}Ni_8Al_{10}$ loaded in uniaxial compression. We show that elastic strain can be determined accurately from the scattering data directly as well as from the resulting pair correlation function. We also observe that the strain in the nearest-neighbor atomic environment is somewhat smaller than the strain measured over longer length scales, but the effect is much smaller than that reported by Poulsen and co-workers.[3] We suggest that the difference in strain between the nearest neighbors and on longer length scales is due to anelastic atomic rearrangements in topologically unstable regions of the glass.

II. BACKGROUND

In a scattering experiment on an isotropic amorphous material, the elastic scattering intensity $I(q)$ is measured as a function of the magnitude of the scattering vector $q = 4\pi \sin\theta/\lambda$, where θ is half of the scattering angle and λ is the wavelength of the radiation. The total structure factor $S(q)$ is then

$$S(q) = \frac{I(q)}{N\langle f(q)\rangle^2}, \tag{1}$$

where N is the number of atoms, $f(q)$ is the atomic scattering factor for x rays, and the angular brackets indicate averaging over the composition of the material.

The real-space structural information available from $S(q)$ is the pair distribution function $\rho(r)$, in which r is the distance from an average atom located at the origin. The pair distribution function is related to $S(q)$ by a Fourier transform,

$$\rho(r) - \rho_0 = \frac{1}{8\pi^3}\int_0^\infty 4\pi q^2[S(q)-1]\frac{\sin qr}{qr}dq, \qquad (2)$$

where ρ_0 is the average atomic density. It is also common to write the real-space structural information in terms of the radial distribution function (RDF), which we define as $4\pi r^2\rho(r)$. With this definition, the coordination number of a particular atomic shell of interest can be obtained by integrating the RDF over a suitably chosen range of r. In what follows we shall use both the RDF and pair correlation function $g(r)=\rho(r)/\rho_0$. The reader should note, however, that there is no general agreement in the literature on terminology for these functions. In particular, Poulsen and co-workers[3] refer to $g(r)$ as the radial distribution function (as do some other authors).

If an amorphous material is subjected to forces that create a macroscopic stress, both $S(q)$ and $g(r)$ will be affected. For the special case of uniaxial loading, the changes in real space are easy to anticipate. A tensile stress will tend to move atoms apart in the loading direction, and hence a peak in $g(r)$ for that direction will move to larger values of r; the opposite will be true for a compressive stress. We can define a strain, analogous to the simple macroscopic definition of engineering strain, as

$$\epsilon = \frac{d_\sigma - d_0}{d_0}, \qquad (3)$$

where d_σ is the position of the peak in $g(r)$ under normal stress σ and d_0 is the position under zero stress. In the transverse direction, we expect a strain of the opposite sign due to the Poisson effect. In the more general case of a multiaxial stress state, the complete strain tensor can be determined from measurement of the strain ϵ in various directions.[1–3]

The situation is not so clear for $S(q)$, even for uniaxial loading. The reciprocal nature of $S(q)$ and $g(r)$ leads us to expect that a tensile stress will tend to cause peaks in $S(q)$ to smaller q. In crystalline materials Bragg's law applies and an individual diffraction peak can be used to unambiguously calculate a particular interplanar spacing. But in amorphous materials there is no such one-to-one correspondence and it is not at all obvious that information about atomic spacings is available directly from the $S(q)$ peak positions. Despite this, it is possible to measure *changes* in atomic spacings—and hence elastic strain—directly from $S(q)$.

To show this, we begin by noting that the scattered intensity from an arbitrary assemblage of atoms averaged over all orientations is given by the Debye scattering equation

$$I(q) = \sum_m \sum_n f_m f_n \frac{\sin qr_{mn}}{qr_{mn}}, \qquad (4)$$

where the sums run over all of the individual atoms and r_{mn} is the distance between atoms m and n. For an amorphous solid, the Debye scattering equation is of limited utility because it requires knowledge of all of the atomic positions. Ehrenfest[4] pointed out, however, that scattering from amorphous materials can be treated in an approximate way by applying Eq. (4) to the case of a diatomic gas, for which coherent scattering between molecules can be neglected. If the atoms are identical, Eq. (4) becomes

$$I(q) = 2f^2\left(1 + \frac{\sin qd}{qd}\right), \qquad (5)$$

where d is the distance between the two atoms. If f is independent of q, then the first maximum of this equation (other than the one at $q=0$) is at $q_{\max}=1.23(2\pi)/d$. One might expect that a similar relation will hold for the case of a condensed material (provided that there is a single predominant interatomic spacing), so we write

$$q_{\max} = \frac{2\pi K}{d}, \qquad (6)$$

where K is a constant that depends on the particular arrangement of the atoms.[5]

Because K can only be determined with a complete knowledge of the atomic positions, Eq. (6) cannot be used to determine the value of d for an amorphous solid directly. But in the case of strain measurements we are interested in changes in d. So if we are willing to assume that the overall change in the structure is sufficiently small that K is independent of the macroscopic stress σ, we can substitute the value of d from Eq. (6) into Eq. (3) to obtain

$$\epsilon = \frac{q_0}{q_\sigma} - 1, \qquad (7)$$

where q_σ and q_0 are the positions of the first peak in $S(q)$ under stress σ and zero stress, respectively. Recently, Yavari and co-workers have used a similar approach to measure changes in free volume as a function of temperature in a $Pd_{40}Ni_{30}Cu_{10}P_{10}$ metallic glass.[6] While still only approximate, these considerations suggest that it is possible to extract strain information directly from changes in $S(q)$. We note that, in general, the peak positions in $I(q)$ will be different from those in $S(q)$, due to the dependence of f on q.

All of the above discussion assumes that the amorphous material is, in fact, isotropic. This is often the case for amorphous alloys, but counterexamples can be found in thin films[7,8] and in bulk alloys subjected to processing that renders them anisotropic.[9] Even in these cases the departure from isotropy is usually small and the scattering data are analyzed using the isotropic assumption. In the present case we also assume that we can neglect the anisotropy induced by the small uniaxial elastic strain, but we note that a full treatment would involve the application of cylindrical distribution functions[10] to properly handle the symmetry.

Poulsen and co-workers[3] provided the first demonstration that the considerations above are essentially correct by measuring elastic strain and strain distributions in amorphous $Mg_{60}Cu_{30}Y_{10}$. They showed that the strain measured according to both Eqs. (3) and (7) increased linearly with uniaxial stress. The strain measured from the position of the first peak in $I(q)$ showed good agreement with strain calculated based on macroscopic measurements of Young's modulus E. However, the strain calculated from $g(r)$ showed a pronounced dependence on r, being the smallest for the first near-neighbor peak and increasing with peaks at higher r to as-

ymptotically approach the strain calculated from the $I(q)$ peak position. The magnitude of the effect was tremendous, with the strain calculated from the third $g(r)$ peak being 2.7 times as large as that from the first peak. Poulsen and coworkers attributed this remarkable observation to unspecified "structural rearrangements on the length scale of 4–10 Å."

In this paper, we report observations that confirm that Eqs. (3) and (7) can be used to measure elastic strain in a metallic glass (and, presumably, other amorphous solids) accurately. We also observe that the strain in the nearest-neighbor shell is smaller than that at longer scales, but the effect is much smaller than that reported by Poulsen and co-workers. We propose that the difference between the stiffness of the nearest-neighbor atomic environment and that over longer length scales can be attributed to the effect of topological rearrangements in the nearest-neighbor environments of a relatively small fraction of the atoms, without the need to invoke significant structural rearrangements over longer length scales.

III. EXPERIMENTAL TECHNIQUES

A. Sample preparation

We produced alloy ingots of nominal composition $Zr_{57}Ti_5Cu_{20}Ni_8Al_{10}$ by arc melting the pure elements under an atmosphere of purified Ar. The ingots were melted several times to improve homogeneity and then suction cast into cylindrical rods 3.2 mm diameter and approximately 75 mm long. The casting procedure is described in more detail elsewhere.[11] After casting, the rods were reduced to a uniform diameter of ~3 mm by centerless grinding and cut to a length:diameter ratio of approximately 2:1 using a low-speed diamond saw. Finally, the ends of the specimen were polished in a special jig to ensure parallelism.

B. *In situ* x-ray scattering experiments

We performed the *in situ* x-ray scattering measurements using monochromatic 80.72-keV (0.0154-nm) x rays at beamline 1-ID of the Advanced Photon Source at Argonne National Laboratory. The beam size was 0.1×0.1 mm^2. We positioned a digital image plate (MAR 345, with a 150 $\times 150$ μm^2 pixel size) 400 mm downstream from the sample to record the scattered intensity in transmission through the cylindrical specimens. A two-dimensional ring pattern was recorded on the image plate. Scattering patterns (intensity versus scattering vector magnitude) were extracted by azimuthally averaging the ring pattern over an arc of approximately 5° centered on the vertical (loading) and horizontal (transverse) directions using the software package FIT2D.[12,13] Data were collected out to a maximum q of approximately 16 Å^{-1}.

Two specimens of nominally identical composition were examined and showed substantially similar behavior; here, we describe the behavior of one specimen in detail. This specimen was loaded incrementally in uniaxial compression in a screw-driven load cell. The loading was paused for approximately 30 min during the x-ray exposures. During each pause, 15 exposures of approximately 10 s duration were collected. The scattering patterns used below were averages of these 15 exposures.

C. Data analysis

Analysis of x-ray scattering data from amorphous materials requires separation of the coherent, elastic, single-scattered x-ray intensity from other scattering contributions and normalization to absolute (electron) scattering units. Although these are standard procedures (see, for instance, Ref. 14), careful attention to them is essential to avoid errors in the determination of the real-space functions $\rho(r)$ or $g(r)$ from the data.

In the present case, there are two circumstances of special note. First, the digital image plate does not discriminate x rays by energy, so x rays resulting from inelastic processes are counted together with the elastically scattered photons. To account for this, we calculated the expected shape of the fluorescence contribution, multiplied it by a suitable scaling factor, and subtracted it from the measured intensity. The scaling factor was chosen based on the quality of the normalization subsequently achieved (see below). We also calculated the Compton scattering intensity in absolute units, corrected it for absorption by the specimen, and subtracted it from the measured intensity as part of the normalization procedure.

The second important factor is the effect of multiple scattering. Often in x-ray scattering experiments it is assumed that multiple scattering is unimportant. If the absorption length is long relative to the sample size, however, double- and higher-order scattering events can contribute significantly to the total measured intensity. This is because the scattering volume for multiple scattering comprises essentially the entire specimen volume, while the single-scattering intensity comes only from that part of the specimen illuminated by the incident beam. To account for this, we calculated the double-scattered x-ray intensity for our cylindrical specimens using a Monte Carlo algorithm to carry out the required numerical integration[15,16] and applied the appropriate correction to the data.[17] Higher-order scattering was neglected.

We applied these corrections, together with the standard corrections for absorption[18] and polarization,[19] to the measured x-ray scattering data. To place the data on an absolute scale, we employed the integral normalization technique of Norman[20] and Krogh-Moe,[21] as well as the large-angle normalization technique of Warren.[22] Agreement between these two techniques, together with the behavior of the resulting structure factor $S(q)$, was used as the criterion for selecting the scaling constant on the fluorescence intensity (see above). Once selected, the same fluorescence scaling constant was used for all of the data sets described here. In all cases, the two normalization techniques yielded normalization constants that differed by less than 0.2%.

IV. RESULTS

A. Reciprocal space

Figure 1 shows the measured structure factor $S(q)$ recorded for the loading direction from 11 x-ray scattering pat-

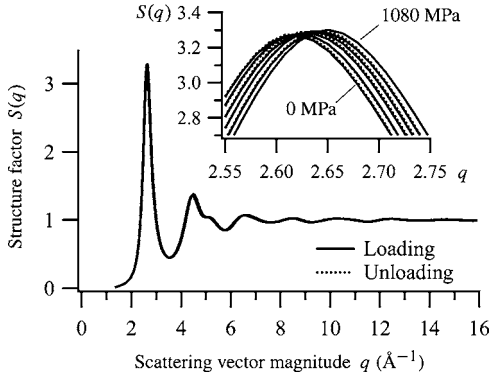

FIG. 1. Structure factor $S(q)$ parallel to the loading direction from 11 scattering patterns collected during incremental loading and unloading. Inset: top of the main peak, showing the shift of the peak in $S(q)$ to larger q with increasing compressive stress.

terns taken at various stresses during incremental loading from 0 MPa to 1080 MPa (approximately 60% of the yield stress for this alloy) and back to zero. As the compressive stress increases, the largest peak in $S(q)$ shifts to larger q in the loading direction. The opposite trend is observed for $S(q)$ in the transverse direction (not shown).

We determined the position of the main peaks in $S(q)$ by fitting the top of the peak to a Gaussian profile and then calculated the strain according to Eq. (7). The results are shown in Fig. 2. The strain increases linearly with increasing compressive stress. A straight-line fit to the data yields an elastic modulus of $E=87\pm2$ GPa, in good agreement with values for E determined by macroscopic measurements on closely related amorphous alloys (Table I). Data for the transverse direction are also shown in Fig. 2; using the strain data from both directions we obtain a value for Poisson's ratio of $\nu=0.34\pm0.01$, also in reasonable agreement with the macroscopic measurements.

In addition to using the $S(q)$ data, we calculated the strain from the change in peak positions in $I(q)$ directly (not shown). We find that the measured strains are equal for both techniques, indicating that the q dependence of $\langle f(q)\rangle^2$ in Eq. (1) is not significant for the small peak shifts that occur due to elastic loading.

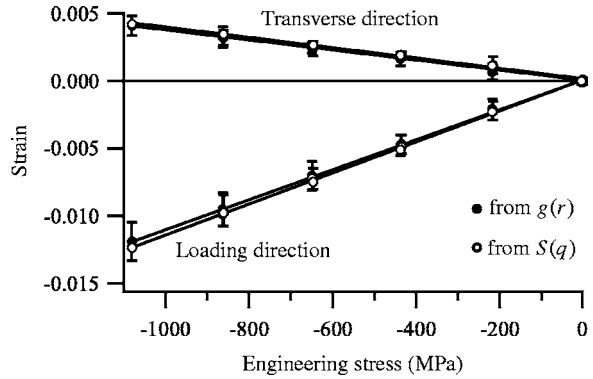

FIG. 2. Strain determined from the structure factor $S(q)$ in reciprocal space and from the pair correlation function $g(r)$ in real space.

TABLE I. Elastic modulus (E) and Poisson's ratio (ν) for several Zr-based bulk metallic glasses.

Alloy	E (GPa)	ν	Reference
$Zr_{57}Nb_5Cu_{15.4}Ni_{12.6}Al_{10}$	86.7	0.38	23
$Zr_{57}Nb_5Cu_{15.4}Ni_{12.6}Al_{10}$	87.3	0.365	24
$Zr_{57}Ti_5Cu_{20}Ni_8Al_{10}$	82.0	0.362	24
$Zr_{50.6}Ti_{5.1}Cu_{18.9}Ni_{11.1}Al_{14.3}$	92.7	0.363	25
$Zr_{53}Ti_5Cu_{20}Ni_{12}Al_{10}$	87.6	0.363	26

B. Real space

The pair correlation functions $g(r)$ for the loading direction obtained by Fourier transformation of the $S(q)$ data collected during the load-unload cycle are shown in Fig. 3. The first peak in $g(r)$ shifts to smaller r with increasing load, as expected, and again the transverse data (not shown) show the opposite trend. In our experience, peak positions in $g(r)$ are difficult to determine accurately because the peaks at low r are asymmetric while those at larger r are rather broad, which leads to significant scatter in the measured strain. A more robust technique is to focus not on the tops of the peaks, but on the places where $g(r)=1$. These crossing points are less sensitive to the effects of asymmetry and can be accurately determined even for peaks at large r.

The strains determined in this way for the loading direction are shown in Fig. 4 for values of r out to $\sim$20 Å at several levels of stress. The strain is approximately independent of r, a point to which we return below. The average strain at each stress was calculated by taking the average (over all r out to 20 Å) from these data and corresponding data for the transverse direction; the results are shown in Fig. 2. Linear fits to the $g(r)$ data in Fig. 2 yield values of $E=90\pm2$ GPa and $\nu=0.33\pm0.01$, in good agreement with the results obtained from the $S(q)$ data.

Although we see no pronounced dependence of strain on r in Fig. 4, it is interesting that the strain determined from the lowest value of r at which $g(r)=1$ is consistently smaller in magnitude than the strains determined at larger values of r. To investigate this further, we examined the behavior of the

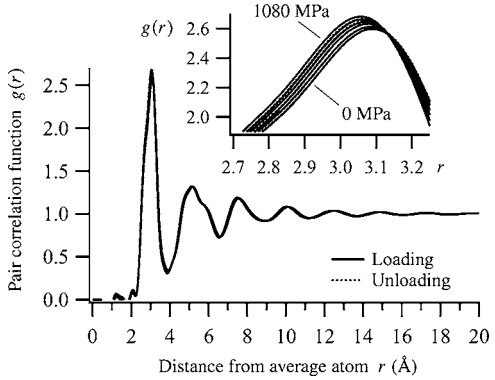

FIG. 3. Pair correlation functions $g(r)$ calculated from the $S(q)$ data in Fig. 1 (parallel to the loading direction). Inset: shift in the first peak in $g(r)$ to smaller r with increasing compressive stress.

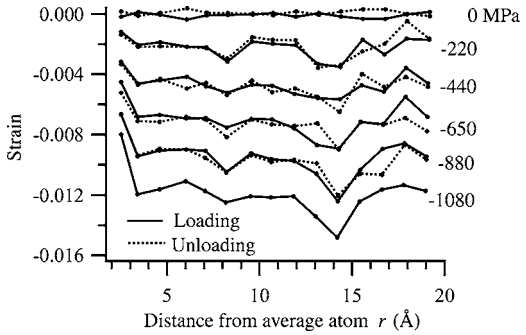

FIG. 4. Strain determined from pair correlation functions $g(r)$ at several stresses.

first peak in the RDF[$4\pi r^2\rho_0 g(r)$, as discussed above]. Figure 5 shows the first peak in the RDF for a representative data set collected at zero stress. In our five-component alloy, this first peak actually consists of 15 overlapping partial pair correlations. The resolution of our experiment does not allow us to distinguish all of these correlations, but they do make the peak asymmetric, and we can fit it to a sum of two Gaussian contributions which we refer to as peak 1 and peak 2. From the fit, the position of peak 1 is 3.133 ± 0.001 Å and the position of peak 2 is 2.661 ± 0.004 Å.

We cannot unambiguously identify the atomic pairs contributing to each of these contributions to the first peak in the RDF, but we can make some reasonable approximations. First, because the contribution of each atomic pair to the RDF is weighted by the atomic scattering factors of the elements and by their concentration, we can neglect the influence of Ti and Al, both of which have low atomic number and are present at relatively low concentration. Second, the separation of the atoms in each pair is related to the sum of their atomic radii; since Cu and Ni are nearly the same size (Table II), their contributions are indistinguishable. So we are left, effectively, with only three pair correlations: Zr-Zr, Zr-(Cu,Ni), and (Cu,Ni)-(Cu,Ni). The expected pair separations (from the respective sums of atomic radii from Table II) along with representative x-ray scattering data from this and closely related amorphous alloys are given in Table III.

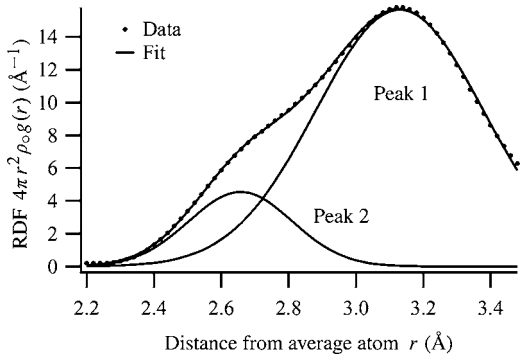

FIG. 5. Radial distribution function $4\pi r^2\rho_0 g(r)$ measured under zero stress, together with the results of a fit to a model consisting of two Gaussian contributions (with no background) over the range of r shown in the figure. (Larger values of r were not included due to the overlapping contribution from the second nearest-neighbor shell.)

TABLE II. Atomic radii for the various elements in $Zr_{57}Ti_5Cu_{20}Ni_8Al_{10}$. These radii are those used by Miracle in Ref. 27 (provided by personal communication).

	Cu	Ni	Al	Ti	Zr
Radius (Å)	1.27	1.28	1.43	1.46	1.58

Based on these results, we conclude that it is reasonable to interpret our peak 1 (at $r=3.133$ Å) as being due primarily to Zr-Zr pairs and our peak 2 (at $r=2.661$ Å) as being due to overlapping (Cu,Ni)-(Cu,Ni) and Zr-(Cu,Ni) pair correlations. Also, the width of peak 2 is approximately half again as large as that of peak 1, supporting the idea that peak 2 has contributions from two distinct types of pair correlations. Identification of the peaks in this way is by no means absolute, but does provide a useful framework for interpreting our results.

Figure 6 shows the strain determined from the shift in the position of these two peaks as a function of stress. The strain determined from peak 1 yields a value of $E=93\pm1$ GPa, slightly larger than that determined from both $g(r)$ and $S(q)$ above (Fig. 2). The strain determined from peak 2 increases much more slowly with stress, yielding a value for $E=149\pm8$ GPa. The difference may related to the inherent stiffness of the particular atomic bonds or to more fundamental differences in how the local atomic environments respond to the stress. This is discussed in more detail below.

In addition to a shift in position, the widths of the two contributions to the first peak in the RDF change during loading. Figure 7 shows the fraction change in full width at half maximum (FWHM) of peaks 1 and 2 in the loading and transverse directions. Together with the change in width, the amplitudes of the peaks in $g(r)$ change with increasing stress (inset to Fig. 3). The changes in width and amplitude offset each other, so that the coordination number of 11.5 ± 0.1 average atoms (defined as the integrated area under the first peak in the RDF for $0\leqslant r\leqslant3.5$ Å) does not change during loading.

V. DISCUSSION

A. Strain measurement

As shown in Fig. 2, elastic strains in metallic glass can be measured accurately by high-energy x-ray scattering. This ability will be useful in the study of metallic-glass-matrix composites, for which several groups have already used x-ray or neutron scattering to measure elastic strains in the crystalline phases.[31–34] It is particularly noteworthy that the elastic strain in the amorphous component can be determined easily from the position of the first peak in $I(q)$, because the presence of strong scattering from the crystalline phase probably precludes reliable determination of $g(r)$. Furthermore, this can be done with relatively short data acquisitions, as there is no need to collect high signal-to-noise-ratio data at high q where the elastic scattering from the amorphous phase is weak [as is required for the Fourier transformation of $S(q)$ to obtain $g(r)$]. Thus, assuming that there is no crystalline

TABLE III. Predicted separation of atomic pairs based on the atomic radii in Table II and data from experiments and simulations for several Zr-based amorphous alloys.

	$r_{(Cu,Ni)-(Cu,Ni)}$ (Å)	$r_{Zr-(Cu,Ni)}$ (Å)	r_{Zr-Zr} (Å)	Reference
Sum of atomic radii	2.55	2.85	3.16	
$Zr_{57}Ti_5Cu_{20}Ni_8Al_{10}$	—	2.68	3.13	28
$Zr_{60}Al_{15}Ni_{25}$	—	2.67	3.17	29
$Zr_{60}Ni_{25}Al_{10}$ (simulation)	2.65	2.63	3.30	30

peak that overlaps the top of the first peak in $I(q)$ from the amorphous component, one should be able to obtain strain information from both phases simultaneously. Experiments of this kind will allow better comparisons with computational models of deformation of metallic-glass-matrix composites.

B. Length-scale dependence of strain

The elastic modulus of a crystalline material reflects the inherent stiffness of the atomic bonds and, in particular, the curvature of the atomic potential energy well.[35] For amorphous alloys, Young's modulus is typically ~30% smaller than that for crystalline phases of similar composition.[36,37] The difference can be attributed to anelastic relaxation events and is not due to a fundamental difference in the atomic bonding, as described in more detail below.

Poulsen and co-workers[3] reported that the elastic strain (and hence the elastic modulus) showed a strong dependence on length scale. In particular, they reported that the strain in the first near-neighbor atomic environment was smaller by a factor of 2.7 than that at large r and that the value at large r was consistent with the strain calculated from macroscopic measurements of Young's modulus. But if the value at large r is consistent with macroscopic measurements and thus roughly 30% smaller than that for a crystalline phase of similar composition, then the much smaller strain for the atomic near neighbors implies that the inherent stiffnesses of the atomic bonds in the nearest-neighbor shell are several times greater in the amorphous alloy than they would be in the corresponding crystalline phases. This seems unlikely.

Our own results (Fig. 4) indicate that the strain as determined from the first peak in $g(r)$ is only slightly smaller than that at higher r. Significantly, the elastic modulus we determine from the shift in the two contributions to the first peak in the RDF (Fig. 6) is quite similar to the macroscopic elastic moduli of the corresponding crystalline phases. For peak 1, which we attribute primarily to Zr-Zr pairs, the measured modulus is 93±1 GPa, which compares well with an elastic modulus of polycrystalline Zr of about 96 GPa (Ref. 38). Similarly, the modulus of 149±8 GPa measured for peak 2, due to overlapping Zr-(Cu,Ni) and (Cu,Ni)-(Cu,Ni) pairs, is on the same order as an average of the elastic moduli of polycrystalline Cu (115 GPa) and Ni (204 GPa), although it is significantly larger than the calculated elastic modulus of tetragonal Zr_2Ni (~49 GPa, Ref. 39). (Interestingly, the shear modulus of evaporated amorphous Ni-Zr thin films as measured by Rubin and Schwarz[40] is approximately twice that of crystalline Zr_2Ni.) These comparisons are only approximate because the uniaxial elastic modulus is a function of the atomic environment as well as the specific atom pairs, but they do suggest that our measurements of the bond stiffnesses in the nearest-neighbor atomic shell are reasonable.

It is, perhaps, not widely appreciated that the microscopic basis of the traditional theory of continuum elasticity is limited to the special case of Bravais lattices, in which every atom is at a center of symmetry.[41] In complex materials this is an area of active research.[42] In granular materials, for instance, it appears that static continuum equations of elasticity only apply at length scales above ~100 particle diameters.[43] Our observation that strain is essentially independent of r for $r>4$ Å (Fig. 4) suggests that length-scale effects of this kind are not significant in metallic glasses beyond the first atomic shell.

C. Elastic and anelastic deformation

The disordered structure of a metallic glass means that atoms exist in a range of local atomic environments; as a

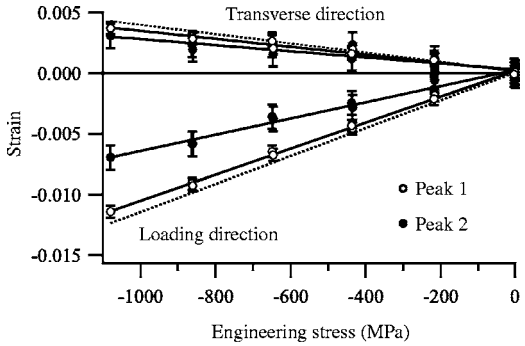

FIG. 6. Strain determined from the positions of the two overlapping peaks in the RDF (Fig. 5). The dotted lines are the strains determined from $S(q)$ (Fig. 2).

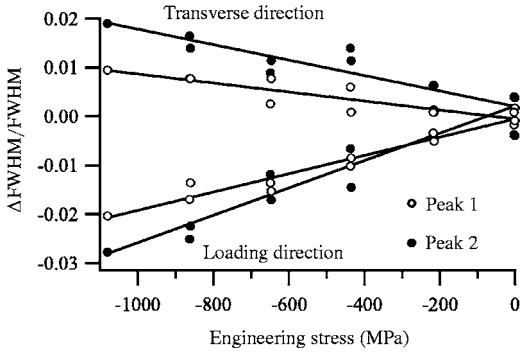

FIG. 7. Change in the widths (FWHM) of the two overlapping peaks in the RDF (Fig. 5).

result, not all atoms (even of the same species) experience the same displacement in elastic deformation. For some atoms, the displacement can be considerably larger than average, leading to an apparent reduction in the elastic modulus. For instance, Weaire and co-workers[44] showed that allowing atomic relaxation in a model calculation reduced the shear modulus by ~33% compared to a model in which no relaxation was permitted. This result suggested that anelastic processes might be occurring during nominally elastic deformation.

Suzuki and Egami[45] explored these atomic relaxations in more detail and showed that they consist of topological rearrangements within the atomic near-neighbor environment in which an atom switches one of its atomic near-neighbors in preference for another atom (originally in the second nearest-neighbor shell). Rearrangements of this type are not possible for most of the atoms in the structure, but can occur in regions where the local dilatation is large enough to render the structure topologically unstable.[46] Because only a small fraction of atoms (approximately 1% for a 1% shear strain[45,46]) participate in these rearrangements, the RDF is not very sensitive to them. Instead, the changes in the first near-neighbor peak of the RDF reflects the purely elastic displacements experienced by the vast majority of the atoms. This explains why the elastic modulus extracted from this shift of this peak is comparable to that of crystalline materials of similar composition. On the other hand, the entire structure gets the benefit of the added deformation due to the atomic rearrangements, so at length scales beyond the first shell the RDF reflects the macroscopic elastic modulus.

Some additional support for this explanation is provided by considering the change in the widths of the peaks in $g(r)$ and the RDF (Figs. 3 and 7) as the macroscopic compressive stress increases. The width of the peaks decreases in the loading direction and increases in the transverse direction, but by a smaller amount. This indicates that the overall effect (averaging over all orientations with respect to the loading direction) is a reduction in peak width with increasing load. Srolovitz and co-workers[47] showed that sharpening of the peaks in $g(r)$ is associated with a decrease in variance of the atomic-level hydrostatic stress distribution, $\langle p^2 \rangle$. Thus, with increasing load the average hydrostatic stress $\langle p \rangle$ increases, but overall p becomes more uniform. Presumably a significant part of the effect we observe comes from the deformation of regions of locally large dilatation, which in the unloaded state are regions of unusually low p. As the load increases, these are the regions in which the atomic rearrangements described above occur. This brings the local p for these regions closer to the overall mean $\langle p \rangle$, thus reducing $\langle p^2 \rangle$ and causing the observed sharpening of the peaks in $g(r)$ and the RDF.

A reduction in $\langle p \rangle$, because it corresponds to a more uniform distribution of free volume, also implies a reduction in the entropy of the glass upon loading. This would imply that the stiffness of metallic glasses (and possibly other amorphous materials) has an entropic component, analogous to the entropic contribution in rubber elasticity.[48]

Finally, we also note that, although we see little length-scale dependence of strain beyond the nearest-neighbor atomic shell, in Fig. 4 the strain in the region around $r = 13-14$ Å is consistently larger in magnitude than that at other values of r. (The effect is small, but it is observed at all loads and in the second sample we examined, as well.) This suggests that the compliance of the glass has an additional contribution from atoms that are, on average, in the fifth or sixth atomic shell around an average atom, again possibly due to a redistribution of free volume. It is interesting to note that this length scale is only slightly larger than the size of shear transformation zones in metallic glasses, currently estimated to be about 10 Å in diameter.[49] This points to a possible link to plastic deformation, as well. We believe that continued exploration of the response of the structure of amorphous alloys under load—closer to the yield stress, for instance, or under different stress states such as tension or pure shear—is likely to yield additional insights.

VI. CONCLUSIONS

The strain in a metallic glass measured by x-ray scattering is in good agreement with macroscopic observations of the elastic behavior of these alloys. Although we do observe a small length-scale dependence of the strain, the effect is much smaller than previously reported and is confined to the nearest-neighbor atomic shell. The strain in this shell yields a modulus that is consistent with the inherent stiffness of the atomic bonds, as measured from crystalline materials of similar composition. These observations are consistent with observations in model calculations that the reduced modulus of metallic glasses (relative to crystalline phases of similar composition) is due to anelastic atomic rearrangements in the nearest-neighbor environment around atoms in topologically unstable regions. We also observe a sharpening of the peaks in the radial distribution function, indicating that the distribution of atomic-level stresses becomes more uniform upon loading. This suggests that the elasticity of metallic glasses may have an entropic component, analogous to the entropic component of rubber elasticity.

ACKNOWLEDGMENTS

We gratefully acknowledge useful discussions with Takeshi Egami, Jonah Erlebacher, K. T. Ramesh, A. Lindsay Greer, and Christopher Schuh; David Dunand and Marcus Young for assistance with the *in situ* loading experiments; and Jonathan Trenkle for assistance with preparing the specimens. T.C.H. and R.T.O. gratefully acknowledge financial support from the U.S. Department of Energy (Grant No. FE-FG02-98ER45699) and the Army Research Laboratory (ARMAC-RTP Cooperative Agreement No. DAAD19-01-2-000315). T.C.H. additionally acknowledges financial support from the National Science Foundation (Grant No. DMR-0307009). Use of the Advanced Photon Source was supported by the U.S. Department of Energy, Office of Science, Office of Basic Energy Sciences, under Contract No. W-31-109-Eng-38.

*Electronic address: hufnagel@jhu.edu
†Present address: Materials and Engineering Physics, Ames Laboratory, Ames, Iowa 50011, USA.

[1] I. C. Noyan and J. B. Cohen, *Residual Stress: Measurement by Diffraction and Interpretation* (Springer-Verlag, New York, 1987).
[2] *Analysis of Residual Stress by Diffraction Using Neutron and Synchrotron Radiation*, edited by M. E. Fitzpatrick and A. Lodini (Taylor & Francis, New York, 2003).
[3] H. F. Poulsen, J. A. Wert, J. Neuefeind, V. Honkimaki, and M. Daymond, Nat. Mater. **4**, 33 (2005).
[4] P. Ehrenfest, Proc. R. Acad. Sci. Amsterdam **17**, 1184 (1915).
[5] A. Guinier, *X-Ray Diffraction in Crystals, Imperfect Crystals and Amorphous Bodies* (Freeman, San Francisco, 1963).
[6] A. R. Yavari, A. L. Moulec, A. Inoue, N. Nishiyama, N. Lupu, E. Matsubara, W. J. Botta, G. Vaughan, M. D. Michiel, and Å. Kvick, Acta Mater. **53**, 1611 (2005).
[7] V. G. Harris, K. D. Aylesworth, B. N. Das, W. T. Elam, and N. C. Koon, Phys. Rev. Lett. **69**, 1939 (1992).
[8] T. C. Hufnagel, S. Brennan, P. Zschack, and B. M. Clemens, Phys. Rev. B **53**, 12024 (1996).
[9] X. Yan, M. Hirscher, T. Egami, and E. E. Marinero, Phys. Rev. B **43**, R9300 (1991).
[10] M. E. Milberg, J. Appl. Phys. **33**, 1766 (1962).
[11] X. Gu, L. Q. Xing, and T. C. Hufnagel, J. Non-Cryst. Solids **311**, 77 (2002).
[12] A. P. Hammersley (unpublished).
[13] A. P. Hammersley, S. O. Svensson, M. Hanfland, A. N. Fitch, and D. Häusermann, High Press. Res. **14**, 235 (1996).
[14] C. N. J. Wagner, J. Non-Cryst. Solids **31**, 1 (1978).
[15] G. D. Wignall, J. A. J. Jarvis, W. E. Munsil, and C. J. Pings, J. Appl. Crystallogr. **7**, 366 (1974).
[16] S. L. Strong and R. Kaplow, Acta Crystallogr. **23**, 38 (1967).
[17] R. Serimaa, T. Pitkänen, S. Vahvaselkä, and T. Paakkari, J. Appl. Crystallogr. **23**, 11 (1989).
[18] A. R. B. Skertchly, Acta Crystallogr. **10**, 535 (1957).
[19] R. Kahn, R. Fourme, A. Gadet, J. Janin, C. Dumas, and D. André, J. Appl. Crystallogr. **15**, 330 (1982).
[20] N. Norman, Acta Crystallogr. **10**, 370 (1957).
[21] J. Krogh-Moe, Acta Crystallogr. **9**, 951 (1956).
[22] B. E. Warren, *X-Ray Diffraction* (Dover, New York, 1990).
[23] R. D. Conner, Y. Li, W. D. Nix, and W. L. Johnson, Acta Mater. **52**, 2429 (2004).
[24] J. Lewandowski, W. Wang, and A. Greer, Philos. Mag. Lett. **85**, 77 (2005).
[25] W. H. Wang, C. Dong, and C. H. Shek, Mater. Sci. Eng., R. **44**, 45 (2004).
[26] Y. X. Wei, B. Zhang, R. J. Wang, M. X. Pan, D. Q. Zhao, and W. H. Wang, Scr. Mater. **54**, 599 (2006).
[27] D. B. Miracle, Nat. Mater. **3**, 697 (2004).
[28] N. Mattern, U. Kühn, H. Hermann, H. Ehrenberg, J. Neuefeind, and J. Eckert, Acta Mater. **50**, 305 (2002).
[29] E. Matsubara, T. Tamura, Y. Waseda, A. Inoue, T. Zhang, and T. Masumoto, Mater. Trans., JIM **33**, 873 (1992).
[30] M. Guerdane and H. Teichler, Phys. Rev. B **65**, 014203 (2002).
[31] D. Dragoi, E. Üstündag, B. Clausen, and M. A. M. Bourke, Scr. Mater. **45**, 245 (2001).
[32] D. K. Balch, E. Üstündag, and D. C. Dunand, Metall. Mater. Trans. A **34**, 1787 (2003).
[33] B. Clausen, S. Y. Lee, E. Üstündag, C. C. Aydiner, R. D. Conner, and M. A. M. Bourke, Scr. Mater. **49**, 123 (2003).
[34] R. T. Ott, F. Sansoz, J. F. Molinari, J. Almer, K. T. Ramesh, and T. C. Hufnagel, Acta Mater. **53**, 1883 (2005).
[35] F. Seitz, *The Modern Theory of Solids* (McGraw-Hill, New York, 1940).
[36] H. S. Chen, J. T. Krause, and E. Coleman, J. Non-Cryst. Solids **18**, 157 (1975).
[37] H. S. Chen, J. Appl. Phys. **49**, 3289 (1978).
[38] G. Simmons, and H. Wang, *Single Crystal Elastic Constants and Calculated Aggregate Properties: A Handbook*, 2nd ed. (MIT Press, Cambridge, MA, 1971).
[39] F. R. Eshelman and J. F. Smith, J. Appl. Phys. **46**, 5080 (1975).
[40] J. B. Rubin and R. B. Schwarz, Phys. Rev. B **50**, 795 (1994).
[41] A. E. H. Love, *A Treatise on the Mathematical Theory of Elasticity* (Dover, New York, 1944).
[42] I. Goldhirsch and C. Goldenberg, Eur. Phys. J. E **9**, 245 (2002).
[43] C. Goldenberg and I. Goldhirsch, Phys. Rev. Lett. **89**, 084302 (2002).
[44] D. Weaire, M. F. Ashby, J. Logan, and M. J. Weins, Acta Metall. **19**, 779 (1971).
[45] Y. Suzuki and T. Egami, J. Non-Cryst. Solids **75**, 361 (1985).
[46] T. Egami, Mater. Sci. Eng., A **A226–228**, 261 (1997).
[47] D. Srolovitz, T. Egami, and V. Vitek, Phys. Rev. B **24**, 6936 (1981).
[48] I. M. Ward, *An Introduction to the Mechanical Properties of Solid Polymers* (Wiley, Chichester, England, 2004).
[49] C. A. Schuh, A. C. Lund, and T. G. Nieh, Acta Mater. **52**, 5879 (2004).